Received November 9, 2020, accepted November 27, 2020, date of publication December 1, 2020,
date of current version December 10, 2020.

Digital Object Identifier 10.1109/ACCESS.2020.3041630

CFD Simulation and Optimization of a Pneumatic Wheat Seeding Device

CHAO WANG[1], HONGWEN LI[1], JINGXU WANG[2], JIN HE[1], QINGJIE WANG[1], AND CAIYUN LU[1]
[1]College of Engineering, China Agricultural University, Beijing 100083, China
[2]College of Mechanical and Electrical Engineering, Wenzhou University, Wenzhou 325035, China

Corresponding author: Hongwen Li (lhwen@cau.edu.cn)

This work was supported by the Program for China Agriculture Research System (CARS-03).

ABSTRACT To improve the performance of pneumatic wheat seeding devices with the goal of achieving pneumatic wheat seeding in soil conditions with high moisture content and heavy clay texture in rice-wheat rotation areas, a simulation optimization study of a pneumatic wheat seeding device was carried out using computational fluid dynamics. In this model, airflow was described by ANSYS Fluent software as a continuous compressible gas phase. The effects of accelerating air pressure, throat distance and nozzle diameter on the steady airflow velocity, the steady airflow length and the inlet 2 negative pressure of airflow field were studied, and a response surface analysis was applied to optimize the pneumatic wheat seeding device. The optimal parameter combination was achieved, which was an acceleration pressure of 700 kPa, a throat distance of 20 mm, a nozzle diameter of 7.2 mm and an acceleration pressure of 700 kPa. Comparative verification results showed that the steady airflow velocity, the steady airflow length and inlet 2 negative pressure of the optimized pneumatic wheat seeding device were 718 m/s, 182 mm and 0.49 kPa by simulations, which were 37%, 3% and 17% greater than those of the original device, respectively. This finding illustrates that the CFD model could describe the characteristics of airflow field well in a pneumatic seeding device and that the regression model for parameter optimization was reliable. Numerical simulation of the airflow field based on CFD approach can provide a theoretical basis for improving the operating performance of a pneumatic seeding device.

INDEX TERMS Wheat, pneumatic seeding device, CFD technology, response surface analysis, airflow field.

I. INTRODUCTION

Wheat is one of the most vital food crops worldwide that is widely adaptable, and its planting area accounts for approximately 30% of global cereal acreage. China has the largest total wheat output in the world, with an annual production of more than 1.3 billion tons [1]. The rice-wheat rotation area that is concentrically distributed in the Yangtze River Basin is one of the main wheat production regions in China, and because of abundant rainfall, high groundwater levels and sticky heavy soil [2], [3], it is suitable for shallow wheat sowing methods that are different from dryland patterns in northern China [4], [5]. However, it is difficult to achieve mechanized wheat seeding because the traditional wheat seeders cannot adapt to soil conditions with a high moisture content and heavy clay texture in rice-wheat rotation fields.

The associate editor coordinating the review of this manuscript and approving it for publication was Amjad Gawanmeh.

In recent years, the poor quality and low efficiency of wheat sowing have improved with the development of specialized seeders for paddy-upland rotation systems. By integrating a strip rotary tillage device, double-disk opener and elastic covering scraper, a broad width and precision minimal-tillage wheat planter could decrease straw blockage and reduce soil adhesion while achieving precision seeding [6]. A 2BMFDC-6 half-tillage seeder applied strip shallow rotary tillage technology to reduce soil adhesion, and showed relatively stable wheat sowing performance in rice stubble field with 20-40% soil moisture content [7]. Happy Seeder, designed by Sidhu *et al.* [8], was able to remove part of the soil and straw that adhered to openers by matching the space position of the rotary blade and openers. Although there are multiple types of wheat seeders for rice-wheat rotation areas, the adhesion phenomenon remains when rotary tillage blades and openers contact sticky heavy soil during field operations, which results in increased operating resistance

and poor sowing quality. Consequently, seeding innovative is required. Compared with traditional seeders, noncontact pneumatic seeding technology accelerated wheat into the soil under a high-speed accelerating airflow without mechanical parts, such as rotary tillers, openers or compacting devices that come into with the soil. Diao *et al.* [9] conducted a preliminary theoretical study on pneumatic seeding technology and proposed a design scheme for pneumatic seeding devices. Pneumatic wheat seeding was realized using a modified gas ejector, and an accelerating tube was added [10]. A preliminary bench experiment indicated that wheat seeds could accelerated into the soil without damage, and different degrees of germination could be achieved in fine-tilled seedbed conditions [11]. Although several basic experiments of noncontact pneumatic seeding technology have been carried out, research on the design of pneumatic seeding devices has been limited, and there have been no studies concerning the application of computational fluid dynamics (CFD) to optimize and analyze pneumatic seeding devices. Specifically the best combination of accelerating gas pressure and key structural parameters can be acquired by investigating detailed jet flow characteristics inside the pneumatic seeding device.

Currently, CFD has been widely used in the field of agricultural engineering, as an effective tool to simulate fluid flow and describe flow fleld characteristics [12]–[14]. Zhang *et al.* [15] employed the CFD method to simulate the fertilizer absorption performance of a low-voltage venturi-injector based on double fertilizer inlets and found that the change in the measured and simulated fertilizer absorption performance with the inlet pressure was highly coincident. Wang *et al.* [16] analyzed the impact of different cross section ratios and inflow pressures on the inspiration capacity and gas-liquid-ratio in terms of the flow field, energy dissipation and vortex intensity using CFD simulations and experimental validation. Dai *et al.* [17] established a three-dimensional steady flow model for the optimization of the airflow distribution chamber of an air-impingement jet dryer, and the simulation results showed little difference compared to the experimental data. To improve the efficiency of water-saving agricultural irrigation systems, a CFD simulation of a round rotatory jet sprinkler was performed by Wang *et al.* [18]. In addition, CFD has been utilized in many analyses to study ejection mechanisms in other agricultural machinery [19]–[22]. The CFD method has been successfully applied to various ejectors, hence it is feasible to optimize the design of a pneumatic seeding device that accelerates wheat with a stable ejecting flow field.

To optimize the pneumatic wheat seeding device, CFD was utilized in this study. The modeling involves the analysis of the velocity field and extraction of the key pressure value. In the simulations, the influences of the accelerating air pressure, throat distance and nozzle diameter on the internal flow field of the pneumatic seeding device were studied in terms of the fluid field, during which the steady airflow velocity, steady airflow length and inlet negative pressure served as simulation test indexes. Finally, a bench experiment of the pneumatic seeding device is performed to verify the simulation optimization results. A theoretical basis for improving the design of pneumatic seeding devices is proposed in this paper.

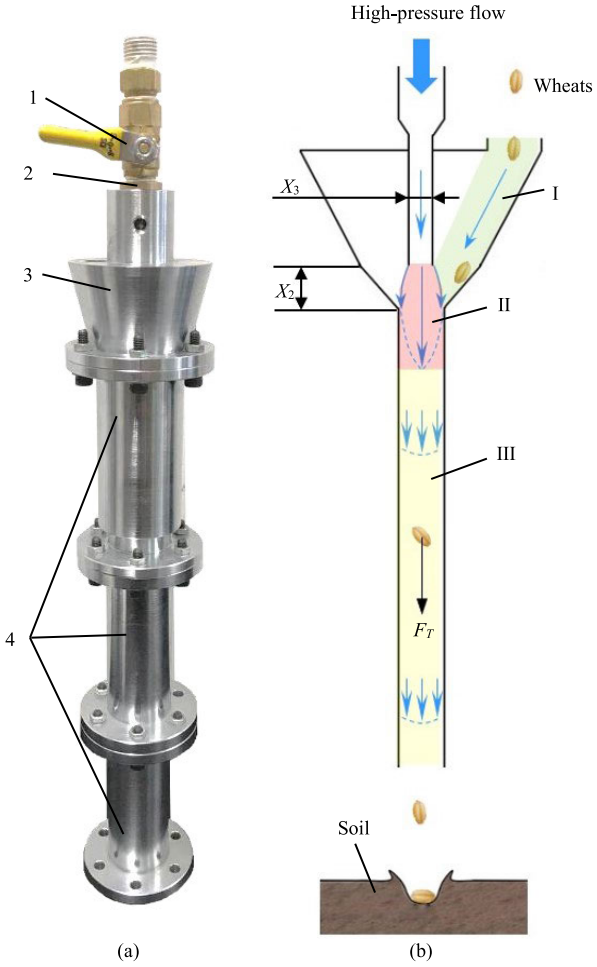

FIGURE 1. Pneumatic Wheat seeding device. (a) Main structure; (b) Working diagram. 1.gas valve; 2.nozzle; 3.ejector base; 4.hybrid accelerating tube.

II. MATERIALS AND METHODS

A. DESCRIPTION OF WHEAT PNEUMATIC SEEDING DEVICE

The pneumatic wheat seeding device was composed of a nozzle, ejector base, hybrid accelerating tube and gas valve, as shown in Fig. 1(a). The nozzle (1) and hybrid accelerating tube (4) were arranged on the top and bottom of ejector base (3), respectively, where the hybrid accelerating tube (4) consisted of three tubular structure components. The working process of the pneumatic seeding device could be divided into 3 stages: the wheat-inhaling process, the wheat and gas mixing process, and the stable wheat accelerating process. As shown in Fig. 1(b), the input high-pressure flow was compressed by the nozzle and then ejected to form the jet stream, under which three different flow regions were

generated in the inner cavity of the pneumatic seeding device: wheat-inhaling zone I, wheat and gas mixing zone II and wheat stable accelerating zone III. Wheat was inhaled into the mixing zone from the seed inlet under the entrainment of the negative pressure flow of the inhaling zone and then pushed into the stable accelerating zone, with steady flow conditions, after blending with the jet stream in the mixing zone. Finally, the wheat flowed out from the bottom of the hybrid accelerating tube and was accelerated into the soil at a certain shooting velocity after accelerating in stable accelerating zone. During pneumatic wheat seeding, stable acceleration of the wheat was produced in the stable accelerating zone, rather than in the mixing zone, the shocked flow field in the mixing zone was unfavorable for speeding up the wheat. Wheat acquired sustained acceleration under the pneumatic thrust force and ignored the effect of gravity in the stable accelerating zone, as shown in Fig. 1(b). The directions of the pneumatic thrust force and relative motion of the wheat were the same. The force acting on the wheat is calculated as the following equation:

$$F_T = C\frac{\pi\rho_g d_m^2}{8}\left(v_g - v_m\right)^2 \tag{1}$$

where F_T is the pneumatic thrust force, ρ_g is the gas density, d_m is the equivalent diameter of the wheat, v_g is the steady airflow velocity of the stable accelerating zone, v_m is the velocity of wheat, and C is the coefficient of the drag force calculated according to Han *et al.* [23].

$$C = \begin{cases} \dfrac{24}{R_e} & (R_e \le 1) \\ \dfrac{24}{R_e}\left(1 + 0.15R_e^{0.657}\right) & (1 < R_e \le 1000) \\ 0.44 & \left(1000 < R_e \le 2 \times 10^5\right) \end{cases} \tag{2}$$

where R_e is the particle's Reynolds number.

The dynamic differential equation [24] of wheat seed in the stable accelerating zone III is expressed as the following equation:

$$\begin{cases} \dfrac{\mathrm{d}v_m}{\mathrm{d}t} = \frac{3C\rho_g}{4d_m\rho_m}\left(v_g - v_m\right)^2 \\ \dfrac{\mathrm{d}l_m}{\mathrm{d}v_m} = \dfrac{4v_m d_m \rho_m}{3C\rho_g\left(v_g - v_m\right)^2} \end{cases} \tag{3}$$

where l_m is the steady acceleration displacement of the wheat, t is the steady acceleration time of the wheat, and ρ_m is the grain density of the wheat.

According to (1) and (3), wheat will obtain a greater speed when the pneumatic thrust force increases by improving the steady airflow velocity in the stable accelerating zone. Therefore, a reasonable internal flow field in the pneumatic seeding device is vital for wheat acceleration and the pneumatic wheat seeding device must be optimized to improve the velocity of the wheat by reducing the length of the mixing zone, improving the length of the stable accelerating zone and increasing steady airflow velocity.

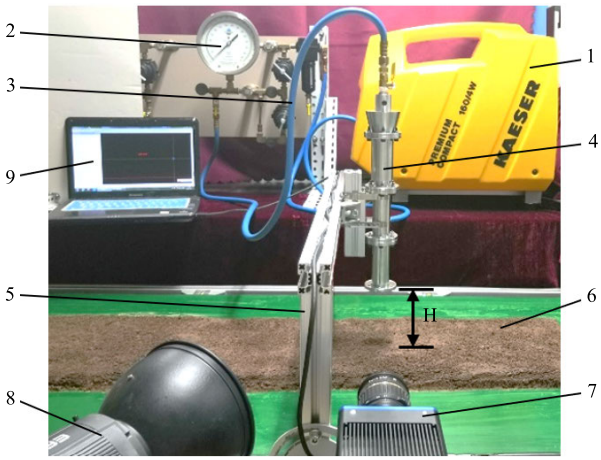

FIGURE 2. Test bench of the pneumatic wheat seeding where the pneumatic seeding height (H), which is the distance between the bottom of the hybrid accelerating tube and the soil surface, is 100 mm. 1. air compressor; 2. pressure regulating device; 3. pressure tubing; 4. pneumatic seeding device; 5. frame; 6. soil; 7. high-speed camera; 8. sunlamp; 9. computer.

B. TEST BENCH OF PNEUMATIC SEEDING DEVICE

After simulation and optimization, comparative studies were conducted on the test bench comparing the original and optimized pneumatic wheat seeding devices (as shown in Fig.2). The device mainly consisted of a frame, pneumatic seeding device, pressure regulating device, pressure tubing, and air compressor. During the test, the pneumatic seeding height between the bottom of the hybrid accelerating tube and the soil surface was 100 mm. The air compressor controlled by a pressure regulating device, provided continuous high-pressure flow that ranged from 0 kPa to 1000 kPa for pneumatic seeding, and high-speed photography was utilized to photograph and analyze the movement of the wheat within pneumatic seeding height H.

C. COMPUTER SIMULATION

1) GEOMETRIC MODELING

The extraction of the computational region and grid features is of critical importance to the results of the flow field analysis [25], [26]. Various three-dimensional pneumatic wheat seeding device model sizes were constructed by using SolidWorks 2016 software, and then the internal cavity was extracted as the computational fluid domain (as shown in Figure 3a) using SCDM 18.2 software. Hexahedron CFD cells meshed by Fluent 18.2 software were employed, and the minimum size limit of the mesh models was 2×10^{-4} m. In addition, five boundary layers were set near the wall, and the density of the nozzle was increased to improve the calculation accuracy. According to the statistics, the minimum orthogonal quality and the maximum aspect ratio of all simulation models were in the range of 0.5-0.6 and 22-32, respectively. The simulation models are shown in Fig. 3b.

2) COMPUTATIONAL CONDITIONS AND PARAMETERS

Airflow was identified as a continuous compressible phase because the flow velocity in the pneumatic wheat seeding

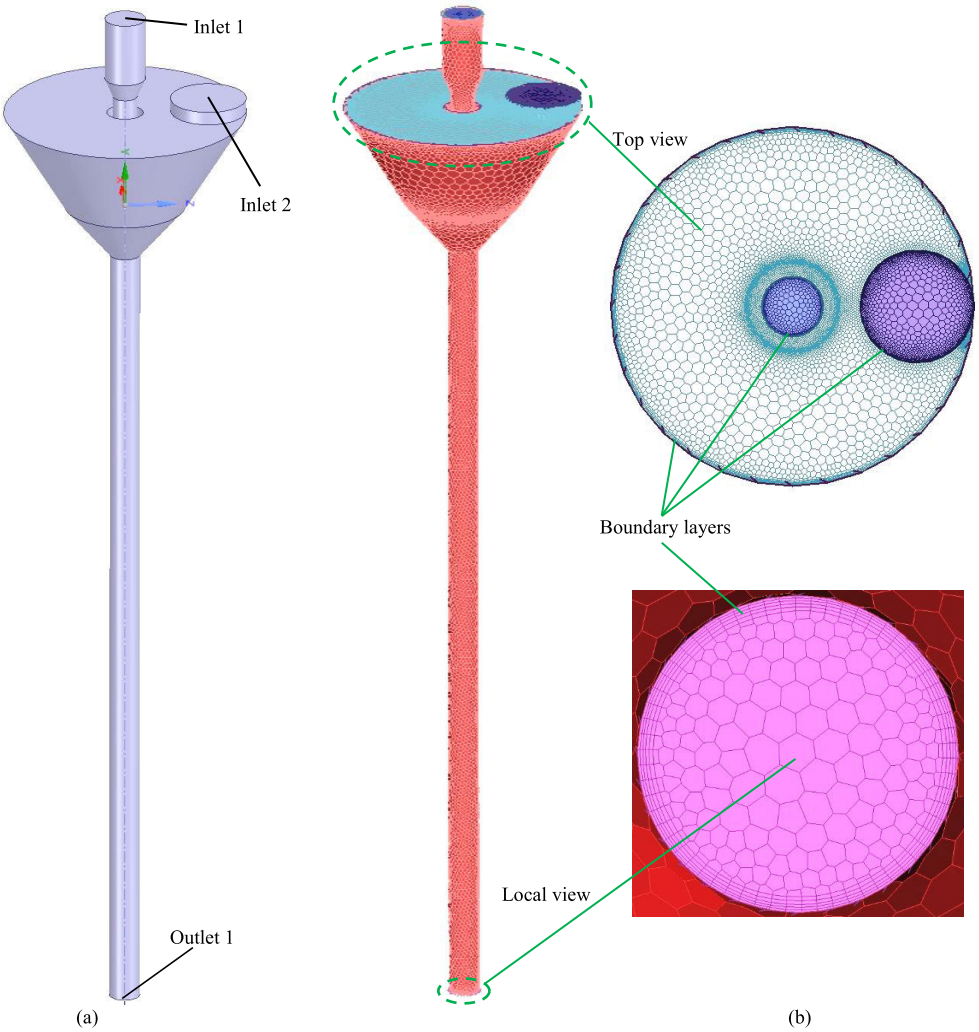

FIGURE 3. Simulation models. (a) Computational region; (b) Computational grids.

device exceeded the speed of sound. Basic control equations in the CFD simulations described by the mass and momentum conservation equation and the energy equation [27] can be expressed as the following equation:

$$\frac{\partial(\rho u_i)}{\partial x_i} = 0 \tag{4}$$

$$\frac{\partial p}{\partial x_i} = \frac{\mu}{3}\frac{\partial}{\partial x_i}\left(\frac{\partial u_k}{\partial x_k}\right) + \mu\frac{\partial^2 u_i}{\partial x_j \partial x_j} + \rho F_i \tag{5}$$

$$\frac{\partial(\rho E + p u_i)}{\partial x_i} = \frac{\partial\left(u_j \tau_{ij}\right)}{\partial x_i} - \frac{\partial q_i}{\partial x_i} \tag{6}$$

where u_i, u_j, and u_k are components of the average flow velocity, and x_i, x_j, and x_k are coordinate components. ρ is the gas density, F_i is the volume force, E is the total energy of the fluid, τ_{ij} is the viscous stress tensor, μ is the gas viscosity, p is the average flow pressure, and q_i is the heat flux term.

The motion of the gas phase was solved with the RNG k-ε turbulence model, which considered the jet characteristics of narrow and long pipes of the pneumatic wheat seeding device. The turbulent kinetic energy equation and turbulent dissipation equation are described as follows:

$$\frac{\partial(\rho k)}{\partial t} + u_i\frac{\partial(\rho k)}{\partial x_i} = \frac{\partial}{\partial x_j}\left(\alpha_k u_{eff}\frac{\partial k}{\partial x_j}\right) + G_k - \rho\varepsilon \tag{7}$$

$$\frac{\partial(\rho\varepsilon)}{\partial t} + u_i\frac{\partial(\rho\varepsilon)}{\partial x_i} = \frac{\partial}{\partial x_j}\left(\alpha_\varepsilon u_{eff}\frac{\partial \varepsilon}{\partial x_j}\right) + \frac{C^*_{1\varepsilon}\varepsilon}{k}G_k - C_{2\varepsilon}\frac{\rho\varepsilon^2}{k} \tag{8}$$

where k is the turbulent kinetic energy, ε is the dissipation rate of turbulent kinetic energy, α_k and α_ε are the Prandtl numbers corresponding to k and ε, μ_{eff} is the equivalent viscosity coefficient, $C^*_{1\varepsilon}$ is a function of the strain rate, $C_{2\varepsilon}$ is an empirical constant, and G_k is the turbulent kinetic energy generation term induced by the mean velocity gradient.

μ_{eff}, $C^*_{1\varepsilon}$ and G_k were defined as follows:

$$\mu_{eff} = \mu + \mu_t \tag{9}$$

$$\mu_t = \rho C_\mu \frac{k^2}{\varepsilon} \tag{10}$$

$$G_k = u_t\left(\frac{\partial u_i}{\partial x_j} + \frac{\partial u_j}{\partial x_i}\right)\frac{\partial u_i}{\partial x_j} \tag{11}$$

TABLE 1. Factors and values for the experiments.

Levels	Factors		
	Accelerating air pressure (kPa) X_1	Throat distance (mm) X_2	Nozzle diameter (mm) X_3
-1	300	10	6
0	500	15	7
1	700	20	8

$$C_{1\varepsilon}^{*} = C_{1\varepsilon} - \frac{\eta\,(1-\eta/\eta_0)}{1+\beta\eta^3} \tag{12}$$

$$\eta = \left(2E_{ij}\cdot E_{ij}\right)^{\frac{1}{2}}\frac{k}{\varepsilon} \tag{13}$$

$$E_{ij} = \frac{1}{2}\left(\frac{\partial u_i}{\partial x_j} + \frac{\partial u_j}{\partial x_i}\right) \tag{14}$$

where C_μ, $C_{1\varepsilon}$ and $C_{2\varepsilon}$ are empirical constants. β is the coefficient of thermal expansion, μ_t is the turbulent viscosity, η is the the ratio of the time scale to the turbulence time, η_0 is the typical value of η in shear flow, and E_{ij} is the average time strain rate.

The finite volume method and second order upwind were utilized to solve the governing equations and the turbulent kinetic energy, respectively. Pressure-velocity coupling was performed using the SIMPLE algorithm. Furthermore, a residual error of 10^{-4} was used to indicate convergence, and the gas velocity of the nozzle was monitored. In setting the boundary conditions, the airflow pressure-inlet at inlet 1 and inlet 2, and the pressure-outlet at outlet 1 were set for all simulations. Both inlet 2 and outlet 1 gauge pressures were 0 kPa, and inlet 1 gauge pressure was the accelerating pressure of the high-speed airflow.

3) OPTIMIZATION DESIGN OF THE PNEUMATIC SEEDING DEVICE

It has been shown that the acceleration pressure X_1, which is the pressure of the high-pressure airflow, the throat nozzle distance X_2 and the nozzle diameter X_3 have significant effects on the internal flow field of pneumatic wheat seeding devices [28], [29]. According to the previous single factor test results [30], the Box-Behnken central composite design from the Design-Expert 8.0.6 software was selected to perform the response surface optimization experiment of the three factors and three levels. The simulation design is shown in Table 1. The accelerating air pressure X_1 consisted of three levels: 300 kPa, 500 kPa and 700 kPa. Three values of throat distance X_2 were included: 10 mm, 15 mm and 20 mm. Three values of the nozzle diameter X_3 were also included: 6 mm, 7 mm and 8 mm. To analyze the influence of the structure and operating parameters and on the working performance of the pneumatic wheat seeding device, regression analyses of the steady airflow velocity Y_1, steady airflow length Y_2, and inlet 2 negative pressure Y_3 were performed under the different parameter combinations. The optimum combination of parameters for the pneumatic wheat seeding device was obtained by regression analysis, and the correlation and interaction between factors were analyzed using the response surface method.

TABLE 2. Simulation design and results.

No.	Accelerating air pressure X_1	Throat distance X_2	Nozzle diameter X_3	Response values		
				Steady airflow velocity (m/s) Y_1	Steady airflow length (mm) Y_2	Inlet2 negative pressure (kPa) Y_3
1	0	0	0	603	186	0.201
2	1	0	1	814	160	0.406
3	0	0	0	604	190	0.208
4	-1	0	1	529	163	0.117
5	0	0	0	603	195	0.209
6	-1	-1	0	467	194	0.124
7	0	0	0	586	189	0.229
8	1	-1	0	718	168	0.313
9	0	1	-1	510	198	0.265
10	-1	1	0	454	168	0.091
11	-1	0	-1	398	187	0.201
12	0	-1	-1	524	188	0.381
13	1	0	-1	612	181	0.513
14	0	0	0	605	196	0.204
15	1	1	0	698	185	0.451
16	0	1	1	662	165	0.306
17	0	-1	1	697	189	0.067

III. RESULTS AND DISCUSSION

There were 17 experimental groups, including 12 groups for the factor analysis experiments and 5 groups for the zero level error estimation experiments. The simulation design and results are shown in Table 2.

A. ESTABLISHMENT OF REGRESSION MODEL

The quadratic polynomial regression model showing the effect of the accelerating air pressure, throat distance and nozzle diameter on the steady airflow velocity, steady airflow length, and inlet 2 negative pressure was established based on the data in Table 2. The regression model is shown in equations (15-17). The variance analysis of regression equations is shown in Table 3.

$$\begin{aligned} Y_1 = {} & 600.2 + 124.25X_1 - 10.25X_2 + 82.25X_3 \\ & - 1.75X_1X_2 + 17.75X_1X_3 - 5.25X_2X_3 \\ & - 12.97X_1^2 - 2.97X_2^2 + 1.02X_3^2 \end{aligned} \tag{15}$$

$$\begin{aligned} Y_2 = {} & 191.2 - 2.25X_1 - 2.87X_2 - 9.63X_3 \\ & + 10.75X_1X_2 + 0.75X_1X_3 - 8.5X_2X_3 \\ & - 12.35X_1^2 - 0.1X_2^2 - 6.1X_3^2 \end{aligned} \tag{16}$$

$$\begin{aligned} Y_3 = {} & 0.21 + 0.14X_1 + 0.029X_2 - 0.058X_3 \\ & + 0.043X_1X_2 - 0.006X_1X_3 + 0.089X_2X_3 \\ & + 0.045X_1^2 - 0.01X_3^2 + 0.055X_3^2 \end{aligned} \tag{17}$$

According to the analysis results in Table 3, the significance levels of the regression model for the steady airflow velocity, steady airflow length and inlet 2 negative pressure were all less than 0.01, implying that the significance of the three regression analysis models was excellent. The significance level of the lack of fit for all regression models was

TABLE 3. Variance analysis of the regression equation.

Source	Steady airflow velocity (m/s) Y_1				Steady airflow length (mm) Y_2				Inlet2 negative pressure kPa (Y_3)			
	Sum of Squares	Freedom	F value	Significant level P	Sum of Squares	Freedom	F value	Significant level P	Sum of Squares	Freedom	F value	Significant level P
Model	1.806E+5	9	473.31	$<0.0001^{**}$	2441.19	9	19.98	0.0003^{**}	0.26	9	118.72	$<0.0001^{**}$
X_1	1.235E+5	1	2912.84	$<0.0001^{**}$	40.50	1	2.98	0.1278	0.17	1	679.98	$<0.0001^{**}$
X_2	840.50	1	19.82	0.003^{**}	66.12	1	4.87	0.0631	6.498E-3	1	26.73	0.0013^{**}
X_3	54120.50	1	1276.43	$<0.0001^{**}$	741.13	1	54.58	0.0002^{**}	0.027	1	110.70	$<0.0001^{**}$
X_1X_2	12.25	1	0.29	0.6076	462.25	1	34.04	0.0006^{**}	7.31E-3	1	30.07	0.0009^{**}
X_1X_3	1260.25	1	29.72	0.0010^{**}	2.25	1	0.17	0.6961	1.323E-4	1	0.54	0.4848
X_2X_3	110.25	1	2.60	0.1509	289.00	1	21.28	0.0024^{*}	0.032	1	129.59	$<0.0001^{**}$
X_1^2	708.84	1	16.72	0.0046^{**}	642.20	1	47.30	0.0002^{**}	8.347E-3	1	34.33	0.0006^{**}
X_2^2	37.27	1	0.88	0.3797	0.042	1	3.101E-3	0.9571	4.19E-4	1	1.72	0.2307
X_3^2	4.42	1	0.10	0.7561	156.67	1	11.54	0.0115^{*}	0.013	1	51.49	0.0002^{**}
Residual	296.80	7			95.05	7			1.702E-3	7		
Lack of Fit	42.00	3	0.14	0.8782	24.25	3	0.46	0.7272	1.219E-3	3	3.37	0.1358
Pure Error	254.80	4			70.80	4			4.828E-4	4		
Cor Total	1.809E+5	16			2536.24	16			0.26	16		

Note: P<0.01 (highly significant, **), P<0.05 (significant, *).

greater than 0.05, indicating that the three regression models had good fitting degrees in the range of the experimental parameters. In addition, the coefficient of determination R^2 of the equations was 0.9985, 0.9625 and 0.9935, demonstrating that more than 96% of the response values could be explained by these three regression models. Therefore, the structural parameters and working parameters of the pneumatic seeding device could be predicted and analyzed using the regression model of the steady airflow velocity, steady airflow length, and inlet 2 negative pressure.

For the main effect, the accelerating air pressure, throat distance and nozzle diameter had highly significant effects on steady airflow velocity and inlet 2 negative pressure, while the nozzle diameter only had a significant effect on the steady airflow length. For the interaction effects, the interactive factor X_1X_3 had a highly significant effect on the steady airflow velocity, and the interactive factor X_1X_2 had a highly significant effect on the steady airflow length and inlet 2 negative pressure. The interactive factor X_2X_3 had a highly significant effect on the steady airflow velocity but had only a significant effect on the inlet 2 negative pressure. For the quadratic factor effect, the quadratic factor X_1^2 had a highly significant effect on steady airflow velocity, steady airflow length and inlet 2 negative pressure. The quadratic factor X_3^2 had a highly significant influence on the steady airflow length and inlet 2 negative pressure. Consequently, the regression models were optimized so that the insignificant items were removed [31], [32] while ensuring $P<0.01$ for the model and $P>0.05$ for the lack of fit, as shown in equations (18-20).

$$Y_1 = 600.2 + 124.25X_1 - 10.25X_2 + 82.25X_3 + 17.75X_1X_3 - 12.97X_1^2 \quad (18)$$

$$Y_2 = 191.2 - 9.63X_3 + 10.75X_1X_2 - 8.5X_2X_3 - 12.35X_1^2 - 6.1X_3^2 \quad (19)$$

$$Y_3 = 0.21 + 0.14X_1 + 0.029X_2 - 0.058X_3 + 0.043X_1X_2 + 0.089X_2X_3 + 0.045X_1^2 + 0.055X_3^2 \quad (20)$$

B. PRIMARY AND SECONDARY IMPACT ANALYSIS OF EACH FACTOR ON THE INDEX

The contribution value rate (K) reflects the influence degree of a single parameter on the regression model such that a higher the value of K indicates a greater the influence degree. K is calculated as follows:

$$\delta = \begin{cases} 0 & F \le 1 \\ 1 - \dfrac{1}{F} & F > 1 \end{cases} \quad (21)$$

$$K_{X_j} = \delta_{X_j} + \frac{1}{2}\sum_{i=1}^{3}\delta_{X_i}\delta_{X_j} + \delta_{X_j^2} \quad j = 1, 2, 3\ i \neq j \quad (22)$$

where δ is evaluation value of the regression term to F, F is each F value of the regression term in the regression equation in Table 3, and K_{Xj} is the contribution rate of each parameter.

From Table 3 and equations (21-22), the order of the contribution rate of each parameter on steady airflow velocity was the accelerating air pressure > nozzle diameter > throat distance. The order of the contribution rate of each parameter on the steady airflow length was nozzle diameter > accelerating air pressure > throat distance. The order of the contribution rate of each parameter on the steady airflow length was nozzle diameter > accelerating air pressure > throat distance. The calculation results are shown in Table 4.

C. EFFECTS OF THE INTERACTIVE FACTORS ON INDEXES

In terms of the above significance analysis, the influence law of the interactive factors X_1X_2, X_1X_3 and X_2X_3 on the steady airflow velocity, steady airflow length and inlet 2 negative pressure were studied.

TABLE 4. Importance of effects of factors on response functions.

Index	Factors contribution rate			Sort contribution rate
	Accelerating air pressure (kPa) X_1	Throat distance (mm) X_2	Nozzle diameter (mm) X_3	
Steady airflow velocity Y_1	2.42	1.46	1.84	$X_1>X_3>X_2$
Steady airflow length Y_2	2.13	1.75	2.37	$X_3>X_1>X_2$
Inlet2 negative pressure Y_3	2.45	2.36	2.47	$X_3>X_1>X_2$

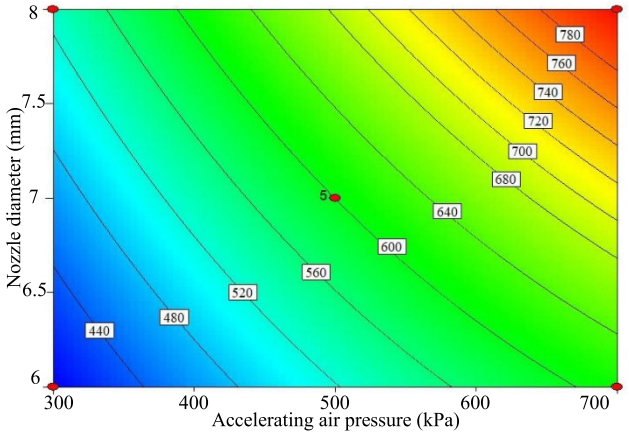

FIGURE 4. Effects of the interactive factors on the steady airflow velocity.

1) EFFECTS OF THE INTERACTIVE FACTORS ON THE STEADY AIRFLOW VELOCITY

At the middle (X_2=15 mm) throat distance, the interaction of the accelerating air pressure and nozzle diameter on the steady airflow velocity is shown in Fig.4. The accelerating air pressure and nozzle diameter were all positively correlated with the steady airflow velocity. The reason for this was that the input energy of the flow field increased as the accelerating air pressure increased, which resulted in an improvement in the output kinetic energy [33]; thus, the steady airflow velocity was increased. Moreover, the output kinetic energy was reduced due to the increasing friction loss when the nozzle diameter decreased, which led to a reduction in the steady airflow velocity. Hence, the expansion of the accelerating air pressure and the nozzle diameter will contribute to an increase in the steady airflow velocity.

2) EFFECTS OF THE INTERACTIVE FACTORS ON THE STEADY AIRFLOW LENGTH

At the middle (X_3 = 7 mm) nozzle diameter, the interaction of the accelerating air pressure and throat distance on the steady airflow length is shown in Fig. 5(a). The steady airflow length first increased and then decreased with an increase in the accelerating air pressure at the same throat distance. There was a negative correlation between the throat distance and the steady airflow length in the accelerating air pressure range of 300-560 kPa and a positive correlation in the range of 560-700 kPa. At the middle (X_3 = 500 kPa) accelerating air pressure, the interaction of the throat distance and nozzle diameter on the steady airflow length is shown in Fig. 5(b). The throat distance had a positive correlation with the steady airflow length for nozzle diameter range of 6-6.7 mm, but had a negative correlation in the nozzle diameter range of 6.7-8 mm. The steady airflow length increased first and then decreased with an increase in the nozzle diameter in a throat distance range of 10-13 mm, and the nozzle diameter had a negative correlation with the steady airflow length when the throat distance was 13-20 mm. The reason for this change was that the high-pressure flow jetted out of the nozzle and expanded to form a jet boundary, as shown in Fig. 6. The maximum steady airflow length could be obtained if the jet flow length L and jet boundary diameter D were equal to the throat distance and the hybrid accelerating tube respectively, otherwise the steady airflow length will be reduced. As the main influencing factor on the jet flow, an increase in the accelerating air pressure and a reduction in the nozzle diameter could extend the jet flow length and narrow the jet boundary diameter. Therefore, there was an optimal combination of the accelerating air pressure [34], throat distance and nozzle diameter that resulted in the maximum stable flow length.

3) EFFECTS OF THE INTERACTIVE FACTORS ON THE INLET 2 NEGATIVE PRESSURE

At the middle (X_3=7 mm) nozzle diameter, the interaction of the accelerating air pressure and throat distance on the inlet 2 negative pressure is shown in Fig. 7(a). The flow entrainment effect was enhanced [35] with increasing accelerating air pressure and throat distance, which continuously improved the inlet 2 negative pressure. At the middle (X_1=500 kPa) accelerating air pressure, the interaction of the throat distance and nozzle diameter on the inlet 2 negative pressure is shown in Fig. 7(b). Jet boundary diameter broadened, with the increasing of nozzle diameter, which enhanced the eddy current effect [36] and decreased the inlet 2 negative pressure over a throat distance range of 10-17 mm. However, the inlet 2 negative pressure showed an increasing trend after decreasing due to the throttling effect for throat distance of 17-20 mm.

IV. OPTIMAZATION AND VERIFICATION

A. PARAMETER OPTIMIZATION

The analysis above indicates that the impact of various factors on the experimental index was inconsistent. To obtain the maximum value of the steady airflow velocity, steady airflow length and inlet 2 negative pressure, a multiobjective optimization method combined with a restraint condition was used to optimize the regression equation. The restraint

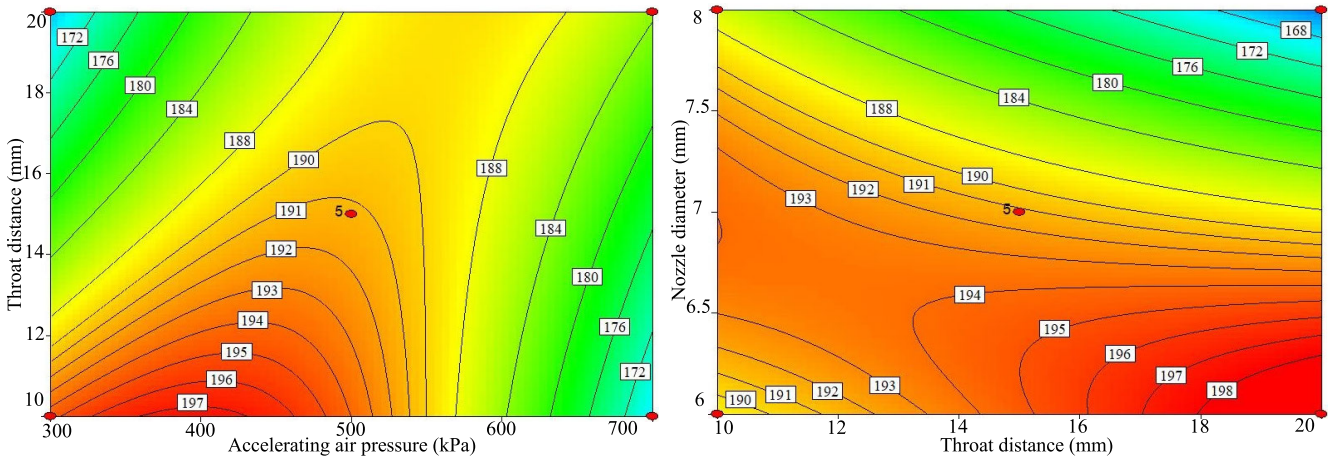

FIGURE 5. Effects of the interactive factors on the steady airflow length. (a) $Y_2 = f(X_1, X_2, 0)$; (b) $Y_2 = f(0, X_2, X_3)$.

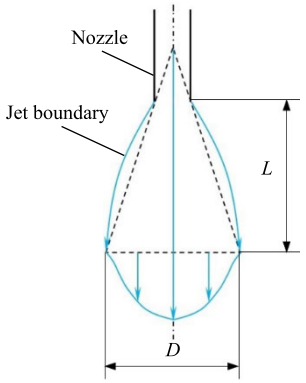

FIGURE 6. Analysis of the nozzle jet flow.

condition is given as:

$$\begin{cases} \max Y_1 \\ \max Y_2 \\ \max Y_3 \\ 300 \le X_1 \le 500 \\ 10 \le X_2 \le 20 \\ 6 \le X_3 \le 8 \end{cases} \tag{23}$$

Equations (18-20) were solved combined with restraint conditions, and the optimal parameter combination was as follows: accelerating pressure was 700 kPa, throat distance was 20 mm and nozzle diameter was 7.2 mm, while the steady airflow velocity was 715 m/s, the steady airflow length was 181 mm and the inlet 2 negative pressure was 0.47 kPa, according to the regression model by simulations.

B. COMPARATIVE VERIFICATION

The velocity contour of the flow field of the original and optimized pneumatic wheat seeding device is shown in Fig.8, where the original parameter combination resulted in an accelerating pressure of 500 kPa, a throat distance of 10 mm and a nozzle diameter of 6 mm. The optimized device had a faster and more stable flow field than the original device in general. Taking the central axis of the wheat pneumatic seeding device as the y-axis, the variation regularity of the velocity and pressure of the central flow field is shown in Fig.9. The airflow velocity increased due to the compression of the nozzle to the high-pressure airflow, and then the airflow velocity presented a downward trend with a slight increase in the pressure due to the air expansion effect after airflow was ejected from the nozzle. Subsequently, the airflow field in the hybrid accelerating tube reached a steady state, and the airflow velocity and pressure remained relatively constant. According to Fig. 9, the steady airflow velocity and steady airflow length of the original device were 524 m/s and 176 mm, respectively, and those of the optimized device were 718 m/s and 182 mm, respectively. The steady airflow velocity increased by 37% whereas the steady airflow length did not obviously change through the optimization of the pneumatic wheat seeding device. When using the optimized parameters, the inlet 2 negative pressure of 0.49 kPa was 17% greater than the original device pressure of 0.42 kPa. Furthermore, there was little difference between the optimized simulation results and the predicted regression model results, which means that the regression model for parameter optimization was accurate.

The wheat pneumatic seeding process obtained using the high-speed photography is shown in Fig.10. High-speed wheat accelerated into the soil after being accelerated in the hybrid accelerating tube. The pneumatic seeding time of the optimized device was 1778 μs, which was 22% shorter than that of the original device at 2286 μs. The decrease of the pneumatic seeding time indirectly demonstrates that the flow field characteristics of the optimized wheat seeding device were better than those of the original device and that the optimized design results were reliable. At the same time, considering the very short wheat seed shooting time of wheat seed, the pneumatic wheat seed seeding process was regarded

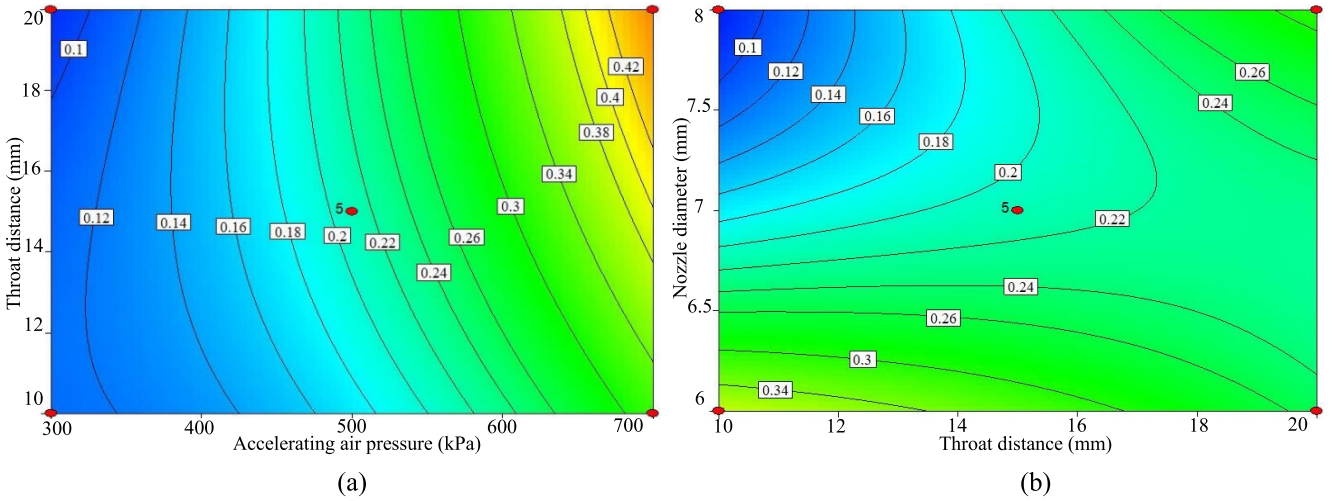

FIGURE 7. Effects of interactive factors on inlet negative pressure. (a) $Y_3 = f(X_1, X_2, 0)$; (b) $Y_3 = f(0, X_2, X_3)$.

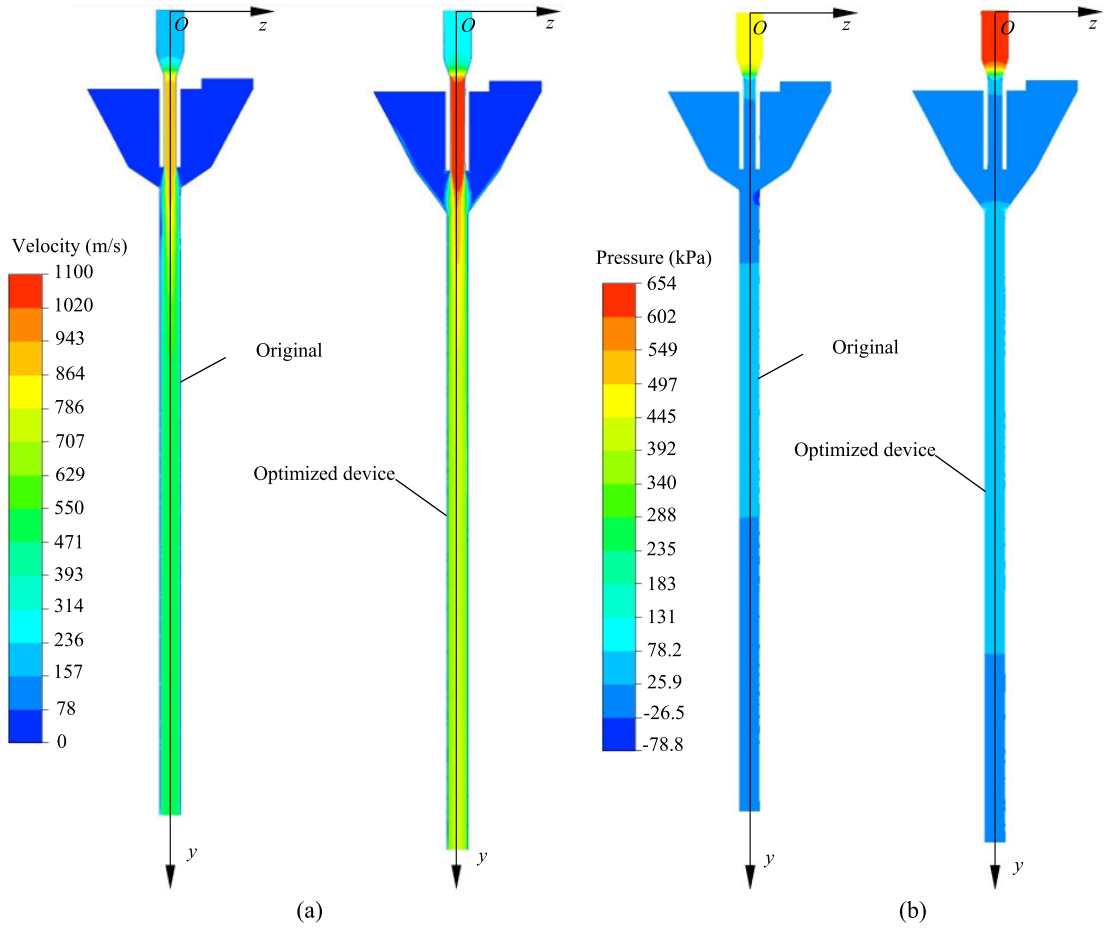

FIGURE 8. Contour plots of the flow field. (a) Velocity contour; (b) Pressure contour.

as uniform shooting. The velocity of the wheat was calculated by the following equation:

$$v_m = \frac{1}{n}\sum_{i=1}^{n}\frac{H}{T_i} \tag{24}$$

where n is the number of wheats pneumatically seeded, and T_i is the pneumatic seeding time of the nth wheat seed.

Using the equations (24) and (2-3), the wheat speed and the actual steady airflow velocity were 56 m/s and 681 m/s for the optimized device, respectively. The actual steady airflow

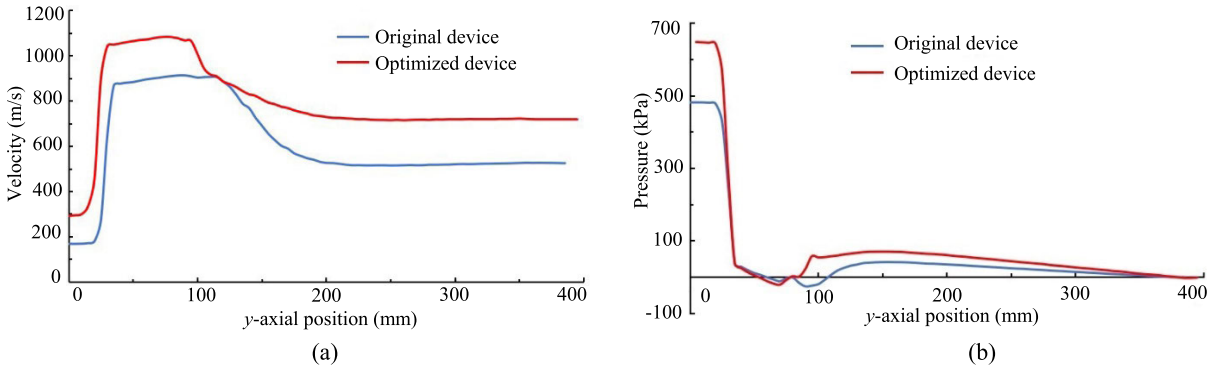

FIGURE 9. Parameter variation curve along the central axis of the flow field. (a) Velocity curve; (b) Pressure curve.

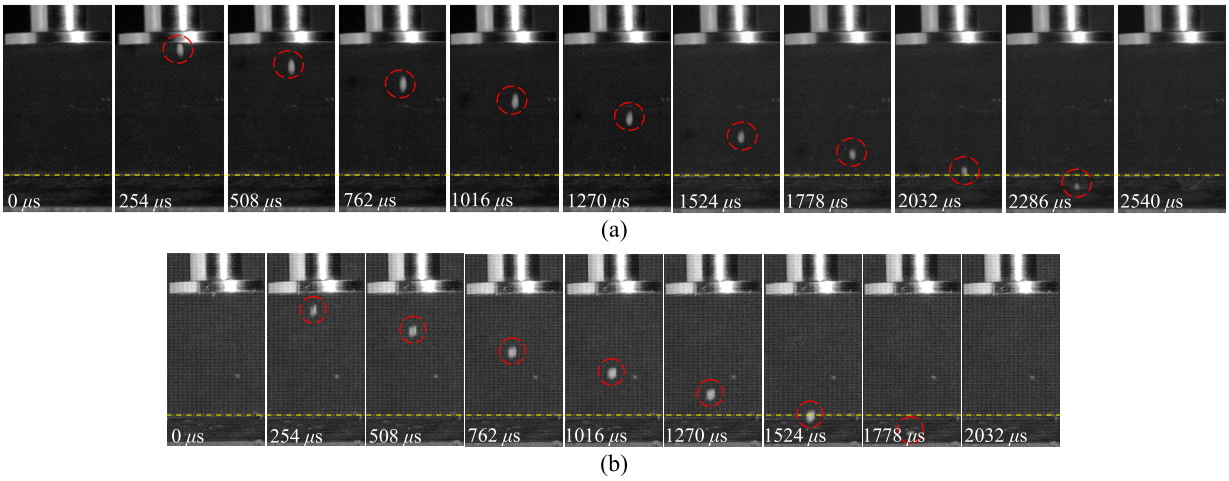

FIGURE 10. Pneumatic wheat seeding process. (a) Pneumatic seeding process of original device; (b) Pneumatic seeding process of the optimized device.

velocity was approximately 5.2% lower than the simulation result, and this result was consistent with the results reported by Wang (2009) [37]and Xu (2012) [38], which indicated that the simulation of the supersonic ejector flow field using the established model was reliable.

C. GERMINATION RESULTS

In the bench experiment, 50 wheat grains were seeded by optimized pneumatic seeding device under the same soil conditions (soil moisture content was 38% and the soil bulk density was 1.25 g/cm^3). In order to observe the effects of the optimized pneumatic seeding device on wheat damage, wheat germination tests with a pneumatic seeding group and a control group without pneumatic seeding were carried out. The wheat germination results were counted after 10 days of culture at approximately 20°C room temperature. The germination rates of the pneumatic seeding group and the control group were 96.0% and 95.3%, respectively, which indicates that sowing wheat seeds into soil using the optimized pneumatic seeding device is feasible and that there was no obvious wheat damage. However, this bench experiment is a basic pneumatic wheat seeding experiment under fine-tilled seedbed conditions without rice straw and stubble mulching. The difference between an experimental soil and field soil that contains impurities, such as stones, crop roots, and soil blocks, should be considered, and pneumatic field seeding experiments should also be carried out to observe and evaluate the effects of pneumatic seeding on wheat seedling emergence, growth and yield.

V. CONCLUSION

In this study, CFD technology was utilized to simulate the effects of the accelerating air pressure, throat distance and nozzle diameter on the steady airflow velocity, steady airflow length and inlet 2 negative pressure of the airflow fleld, and then, response surface analysis was applied to optimize the study of a pneumatic wheat seeding device. The CFD model could describe the characteristics of the airflow field well in a pneumatic seeding device, and the regression model could also adequately guide the optimization of the pneumatic wheat seeding device, leading to the following conclusions:

(1) Via a response surface optimization experimental design and an analysis of the flow characteristics of the airflow field, the primary and secondary factors affecting the working performance of the pneumatic wheat seeding device were assessed. The optimal parameter combination

was achieved: an acceleration pressure of 700 kPa, a throat distance of 20 mm, a nozzle diameter of 7.2 mm and an acceleration pressure of 700 kPa. These values were determined by the simulation regression model.

(2) The velocity and pressure variation regularity of the central flow field was obtained. The airflow velocity was increased by compressing the nozzle to achieve high-pressure airflow, and then, the airflow velocity showed a downward trend with a slight increase in the pressure due to the air expansion effect after ejection from the nozzle. Subsequently, the airflow field in the hybrid accelerating tube reached steady state, and the airflow velocity and pressure remained relatively constant. The ejection function of the pneumatic wheat seeding device could be realized after optimization.

(3) The steady airflow velocity, steady airflow length and inlet 2 negative pressure of the optimized wheat pneumatic seeding device were 718 m/s, 182 mm and 0.49 kPa, which were 37%, 3% and 17% greater than those of the original device, respectively. There was little difference between the optimized simulation values and the predicted regression model values, which meant that the regression model for the parameter optimization was accurate. In addition, the pneumatic seeding time of optimized device was 22% shorter than that of the original device, which also demonstrates that the optimized design results were reliable.

The CFD model was utilized to better understand the airflow field of a pneumatic wheat seeding device and to optimize the operational and structural parameters when combined with a regression model. The model has been shown to be reliable as a tool for understanding the physical phenomenon of airflow and can be applied to analyze the sources of differences. Simulation of the airflow field based on CFD technology and response surface analysis can improve the working performance of pneumatic wheat seeding devices.

REFERENCES

[1] R. J. Qiu, Z. Yang, Y. Jing, C. Liu, and Z. Wang, "Analysis of water and heat flux over rice-wheat rotation field and influencing factors," *Trans. Chin. Soc. Agricult. Eng.*, vol. 34, no. 17, pp. 82–88, 2018.

[2] H. B. Zhu, "Study on anti-blocking device of no-till wheat planter for broken and crushing rice crop stubble," Ph.D. dissertation, Dept. Beijing, China Agri. Univ., Beijing, China, 2013.

[3] Q. Jing, H. V. Keulen, and H. Hengsdijk, "Modeling biomass, nitrogen and water dynamics in rice–wheat rotations," *Agricult. Syst.*, vol. 103, no. 7, pp. 433–443, Sep. 2010.

[4] B. W. J. X. Z. J. M. X. P. Li and W. J. Xu, "Design of GBSL-180 seeder with two-axel rotary tillaging and stubble cleaning," *Trans. Chin. Soc. Agricult. Eng.*, vol. 39, pp. 180–182, Mar. 2008.

[5] C. S. Li, Y. L. Tang, C. Wu, and G. Huang, "Effect of sowing patterns on growth, development and yield formation of wheat in rice stubble land," *Trans. Chin. Soc. Agricult. Eng.*, vol. 28, pp. 36–43, Jan. 2012.

[6] H. Hu, H. Li, C. Li, Q. Wang, J. He, W. Li, and X. Zhang, "Design and experiment of broad width and precision minimal tillage wheat planter in rice stubble field," *Trans. Chin. Soc. Agricult. Eng.*, vol. 32, no. 4, pp. 24–32, 2016.

[7] C. S. Li, Y. Tang, L. Xie, G. Huang, G. Zhong, C. Wu, and S. Cheng, "Design and experiment of 2BMFDC-6 half-tillage seeder of wheat after rice," *Southwest Chin. J. Agri. Sci.*, vol. 24, no. 2, pp. 789–793, 2011.

[8] H. S. Sidhu, E. Humphreys, S. S. Dhillon, J. Blackwell, and V. Bector, "The happy seeder enables direct drilling of wheat into rice stubble," *Austr. J. Experi. Agri.*, vol. 47, no. 7, pp. 844–854, 2007.

[9] P. S. Diao, R. C. Du, Z. D. Yang, and S. D. Yang, "Theoretical research on pneumatic seeding," *J. Agri. Mechan. Res.*, vol. 27, pp. 94–96, Jan. 2005.

[10] Wang C, Li H W, He J, and, "Effect of incident angle on wheat soil-ripping parameters by pneumatic seeding," *Transact. Chin. Soc. Agri. Eng.*, vol. 35, pp. 32–39, 2019.

[11] Wang Y B, Li H W, Wang Q J, and, "Design and experiment of wheat mechanical shooting seed-metering device," *Transact. Chin. Soc. Agri. Eng.*, vol. 51, pp. 101–112, 2020.

[12] S. Gao, K. Cheng, S. Chen, H. Ding, and H. Fu, "CFD based investigation on influence of orifice chamber shapes for the design of aerostatic thrust bearings at ultra-high speed spindles," *Tribol. Int.*, vol. 92, pp. 211–221, Dec. 2015.

[13] J. Huang, T. Wang, T. C. Lueth, J. Liang, and X. Yang, "CFD based investigation on the hydroplaning mechanism of a Cormorant's webbed foot propulsion," *IEEE Access*, vol. 8, pp. 31551–31561, 2020.

[14] J. Jiang and Z. Liu, "The experimental and CFD research on the pressure reduction process of the double rotor hydraulic transformer," *IEEE Access*, vol. 7, pp. 91569–91581, 2019.

[15] J. K. Zhang, J. Li, H. Wu, Z. Ma, E. Waleed, and H. Hu, "Design and experiment of low pressure Venturi injector based on double fertilizer inlets," *Trans. Chin. Soc. Agricult. Eng.*, vol. 33, no. 14, pp. 115–121, 2017.

[16] Y. Wang, Y. Han, X. Zhu, W. Sun, P. Cao, and W. Wu, "Optimization and experiment on performance of flow-ejecting self-priming pump based on CFD," *Trans. Chin. Soc. Agricult. Eng.*, vol. 32, no. 1, pp. 16–21, 2016.

[17] J. W. Dai, H. Xiao, J. Bai, Q. Zhang, L. Xie, and Z. Gao, "Numerical simulation and optimum design on airflow distribution chamber of air-impingement jet dryer," *Trans. Chin. Soc. Agricult. Eng.*, vol. 29, no. 3, pp. 69–76, 2013.

[18] W. Xinkun, X. Shengrong, F. Erdong, Y. Jicheng, and J. Binbin, "Structure design and hydraulic performance test of round rotatory jet sprinkler," *Trans. Chin. Soc. Agricult. Eng.*, vol. 50, pp. 132–137, Feb. 2019.

[19] I. W. Eames, A. E. Ablwaifa, and V. Petrenko, "Results of an experimental study of an advanced jet-pump refrigerator operating with R245fa," *Appl. Thermal Eng.*, vol. 27, nos. 17–18, pp. 2833–2840, Dec. 2007.

[20] J. Fan, J. Eves, H. M. Thompson, V. V. Toropov, N. Kapur, D. Copley, and A. Mincher, "Computational fluid dynamic analysis and design optimization of jet pumps," *Comput. Fluids*, vol. 46, no. 1, pp. 212–217, Jul. 2011.

[21] K. Svensson, P. Rohdin, and B. Moshfegh, "A computational parametric study on the development of confluent round jet arrays," *Eur. J. Mech. B/Fluids*, vol. 53, pp. 129–147, Sep. 2015.

[22] C. Wang, J. B. Zhu, and B. Hu, "Suction performance and energy dissipation characteristics of annular submerged jets," *Trans. Chin. Soc. Agricult. Eng.*, vol. 47, no. 8, pp. 14–21, 2016.

[23] D. Han, D. Zhang, H. Jing, L. Yang, T. Cui, Y. Ding, Z. Wang, Y. Wang, and T. Zhang, "DEM-CFD coupling simulation and optimization of an inside-filling air-blowing maize precision seed-metering device," *Comput. Electron. Agricult.*, vol. 150, pp. 426–438, Jul. 2018.

[24] N. I. I. Hewedy, M. H. Hamed, F. S. Abou-Taleb, and T. A. Ghonim, "Optimal performance and geometry of supersonic ejector," *J. Fluids Eng.*, vol. 130, no. 4, Apr. 2008, Art. no. 041204.

[25] J. Jiang, C. Liu, and B. Yu, "Modeling and simulation for pressure character of the plate-inclined axial piston type hydraulic transformer," in *Proc. IEEE Int. Conf. Inf. Autom.*, Jun. 2010, pp. 245–249.

[26] X. Lei, Y. Liao, and Q. Liao, "Simulation of seed motion in seed feeding device with DEM-CFD coupling approach for rapeseed and wheat," *Comput. Electron. Agricult.*, vol. 131, pp. 29–39, Dec. 2016.

[27] T. Y. Zhang, "Design and optimization of stamping and ejecting device for air cooling system of aircraft," Ph.D. dissertation, Dept. Nanjing Aero. Astro. Univ., Nanjing, Nanjing, China, 2018.

[28] C. Wang, C. Lu, H. Li, J. He, Q. Wang, and X. Cheng, "Preliminary bench experiment study on working parameters of pneumatic seeding mechanism for wheat in rice-wheat rotation areas," *Int. J. Agricult. Biol. Eng.*, vol. 13, no. 1, pp. 66–72, 2020.

[29] S. Varga, A. C. Oliveira, X. Ma, S. A. Omer, W. Zhang, and S. B. Riffat, "Experimental and numerical analysis of a variable area ratio steam ejector," *Int. J. Refrig.*, vol. 34, no. 7, pp. 1668–1675, Nov. 2011.

[30] W. Chao, L. Hongwen, H. Jin, W. Qingjie, L. Caiyun, and W. Jingxu, "Design and experiment of pneumatic wheat precision seed casting device in rice-wheat rotation areas," *Trans. Chin. Soc. Agricult. Eng.*, vol. 51, pp. 43–53, May 2020.

[31] S. M. Ding, X. Xue, J. Fang, Z. Sun, C. Cai, L. Zhou, and W. Qin, "Parameter optimization and experiment of air-assisted pollination device," *Trans. Chin. Soc. Agricult. Eng.*, vol. 31, no. 8, pp. 68–75, 2015.

[32] G. Palermo, C. Silvano, and V. Zaccaria, "ReSPIR: A response surface-based Pareto iterative refinement for application-specific design space exploration," *IEEE Trans. Comput.-Aided Design Integr. Circuits Syst.*, vol. 28, no. 12, pp. 1816–1829, Dec. 2009.
[33] A. Hemidi, F. Henry, S. Leclaire, J.-M. Seynhaeve, and Y. Bartosiewicz, "CFD analysis of a supersonic air ejector. Part I: Experimental validation of single-phase and two-phase operation," *Appl. Thermal Eng.*, vol. 29, nos. 8–9, pp. 1523–1531, Jun. 2009.
[34] I. W. Eames, "A new prescription for the design of supersonic jet-pumps: The constant rate of momentum change method," *Appl. Thermal Eng.*, vol. 22, no. 2, pp. 121–131, Feb. 2002.
[35] D. Chong, M. Hu, W. Chen, J. Wang, J. Liu, and J. Yan, "Experimental and numerical analysis of supersonic air ejector," *Appl. Energy*, vol. 130, pp. 679–684, Oct. 2014.
[36] T. Sriveerakul, S. Aphornratana, and K. Chunnanond, "Performance prediction of steam ejector using computational fluid dynamics: Part 1. Validation of the CFD results," *Int. J. Thermal Sci.*, vol. 46, no. 8, pp. 812–822, Aug. 2007.
[37] H. X. Wang, "The design and numerical simulation of ejector," M.S. thesis, Dept. Energy Power, Nanjing Sci., Tech. Univ., Nanjing, China, 2009.
[38] X. Xu, "Study of the flow phenomenon and design method of ejector," M.S. thesis, Dept. Power Eng., Huazhong Sci., Tech. Univ., Wuhan, China, 2012.

CHAO WANG was born in 1991. He is currently pursuing the Ph.D. degree with the College of Engineering, China Agriculture University, Beijing, China. His current research interests include wheat seeding, conservation agriculture, and computational fluid dynamics.

HONGWEN LI was born in 1968. He received the Ph.D. degree from the College of Engineering, China Agriculture University, Beijing, China, in 1995. He is currently a Chair Professor of Cheung Kong Scholars Programme and the Director of the China Institute for Conservation Tillage. He has undertaken and finished many national research projects in recent years. He had published over 200 articles in local and international journals and six professional books. His current research interests include conservation tillage, modern agricultural equipment, and computer measurement and control.

JINGXU WANG was born in 1987. She received the Ph.D. degree from the College of Engineering, China Agriculture University, Beijing, China, in 2016. She is currently a Lecturer with the Mechanical and Electrical Engineering College, Wenzhou University, Wenzhou, China. Her current research interests include precision seeding, modern agricultural equipment, and conservation tillage.

JIN HE was born in 1979. He received the Ph.D. degree from the College of Engineering, China Agriculture University, Beijing, China, in 2007. He is currently the Vice President of the China Institute for Conservation Tillage. He has undertaken and finished many national research projects in recent years. He had published over 160 articles in local and international journals and three professional books. His current research interests include conservation tillage, modern agricultural equipment, and computer measurement and control.

QINGJIE WANG was born in 1979. He received the Ph.D. degree from the College of Engineering, China Agriculture University, Beijing, China, in 2009. He is currently the Vice President of the College of Engineering, China Agriculture University. He has undertaken and finished many national research projects in recent years. He had published over 130 articles in local and international journals and three professional books. His current research interests include conservation tillage, modern agricultural equipment, and computer measurement and control.

CAIYUN LU was born in 1986. She received the Ph.D. degree from the College of Engineering, China Agriculture University, Beijing, China, in 2014. She is currently an Associate Professor with the College of Engineering, China Agriculture University. She has undertaken Beijing Natural Science Foundation and Ministry of agriculture and rural projects in recent years. She had published over 35 articles in local and international journals and three professional books. Her current research interests include conservation tillage, modern agricultural equipment, and computer measurement and control.